

## Hard and superhard nanolaminate and nanocomposite coatings for machine elements based on Ti6Al4V alloy

**B. Wendler** <sup>a,\*</sup>, **T. Moskalewicz** <sup>b</sup>, **I. Progalskiy** <sup>a</sup>, **W. Pawlak** <sup>a</sup>, **M. Makówka** <sup>a</sup>,  
**K. Włodarczyk** <sup>a</sup>, **P. Nolbrzak** <sup>a</sup>, **A. Czyrska-Filemonowicz** <sup>b</sup>, **A. Rylski** <sup>a</sup>

<sup>a</sup> Institute of Materials Science and Engineering, Lodz University of Technology,  
ul. Stefanowskiego 1/15, 90-924 Łódź, Poland

<sup>b</sup> Department of Metallurgy & Industrial Information Technology, AGH-University  
of Science & Technology, Al. A. Mickiewicza 30, 30-059 Kraków, Poland

\* Corresponding author: E-mail address: bowe@p.lodz.pl

Received 26.09.2010; published in revised form 01.11.2010

### Manufacturing and processing

#### ABSTRACT

**Purpose:** Verification of a series of hybrid treatments of Ti6Al4V alloy consisting of primary diffusion hardening of the substrate with subsequent deposition of wear resistant coatings.

**Design/methodology/approach:** Different nanolaminate and nanocomposite coatings were deposited with use of four different methods including a newly developed high density gas pulsed plasma MS technique. After deposition the coatings were investigated using OM, SEM, HRTEM, XRD, XPS, nanoindentation, Daimler-Benz, ball-on-plate and scratch tests.

**Findings:** Besides an important increase of Ti6Al4V alloy hardness much greater further increase of hardness was obtained due to coatings deposition up to 53 GPa in case of a nanolaminate coating and to 47 GPa in case of a nanocomposite nc-TiN/a-SiN coating. At the same time the volume wear coefficient decreases several orders of magnitude for all the coatings. Simultaneously the friction coefficient decreased to a great extent except for the nc-TiN/a-SiN coating.

**Research limitations/implications:** High density gas pulsed plasma magnetron sputtering is an effective method for superhard coatings deposition, however the roughness of the deposited nc-TiN/a-SiN coating was greater than after conventional magnetron sputtering. This finding needs further experimental and theoretical investigation.

**Practical implications:** Greater surface roughness and high resistance to wear of the coatings synthesized using the newly developed gas pulsed plasma magnetron sputtering deposition limits their application to wear protection of cutting tools rather than for friction reduction in tribological couples.

**Originality/value:** Applicability of the broad spectrum of nanolaminate and nanocomposite coatings as well as different CVD and PVD techniques for an improvement of tribological properties of Ti6Al4V alloy was analyzed in the paper including a newly developed original high density gas pulsed plasma magnetron sputtering technique.

**Keywords:** Superhard coating; Nanolaminate; Nanocomposite; Friction reduction, Resistance to wear; FCAE; PCAD

#### Reference to this paper should be given in the following way:

B. Wendler, T. Moskalewicz, I. Progalskiy, W. Pawlak, M. Makówka, K. Włodarczyk, P. Nolbrzak, A. Czyrska-Filemonowicz, A. Rylski, Hard and superhard nanolaminate and nanocomposite coatings for machine elements based on Ti6Al4V alloy, Journal of Achievements in Materials and Manufacturing Engineering 43/1 (2010) 455-462.

## 1. Introduction

In order to improve much more the load-carrying capacity (higher than 1 GPa) and the tribological properties of Ti alloys, as well as to decrease their proneness to seizure and dry friction coefficient against a majority of important technical alloys, a multiplex treatment was proposed, in which a gradient  $TiC_xNy$  layer with superficial low friction, hydrogenated diamond-like a-C:H coating, was deposited onto an enhanced diffusion-hardened surface of a titanium alloy substrate [1]. Yetim et al. [2] proposed a series of plasma diffusion treatments of the Ti6Al4V alloy including oxidizing, nitriding and oxynitriding, with effective decrease of the wear rate, however with a friction coefficient greater than 0.3. Voevodin et al. [3] in their review article gave a broad spectrum of modern hard, tough and low friction, functionally graded or nanolaminate (i.e., nanostructured in one dimension) or nanocomposite coatings (i.e., nanostructured in three dimensions) on different substrates. Yang et al. [4] demonstrated the excellent tribological properties of magnetron sputtered a-C coatings. Czyżniewski [5] showed useful tribological properties under dry sliding conditions of carbon-based nanocomposite coatings nc-WC/a-C and nc-WC/a-C:H. Wendler et al. [6] proposed another low friction nanocomposite nc-WC<sub>1-x</sub>/a-C coating. Zehnder and Patscheider [7], Pei et al. [8] and Lin et al. [9] proved that nanocomposite nc-TiC/a-C and nc-TiC/a-C:H coatings deposited onto Si, AISI 304 stainless steel and high chromium X120CrW12 tool steel by means of a closed field unbalanced magnetron sputtering ion plating (CFUBMSIP) method protect well these substrates against wear and decrease effectively the dry friction coefficient. Gassner et al. [10] showed that hydrogenated nanocomposite coatings nc-CrC/a-C:H deposited by a direct-current magnetron sputtering onto Si, low alloyed carbon steel DC01 and 6-5-2 high speed (HS) steel can decrease the friction coefficient of dry sliding to a value of 0.05. Pawlak et al. [11] proposed a number of multilayer, hybrid tribological coatings onto Ti6Al4V alloy. Batory et al. [12] proposed a low stress, friction reducing, gradient a-C:H(Ti) coating onto titanium alloy substrates. Włodarczyk et al. [13] proposed a number of low friction and wear resistant, nanocomposite, hydrogenated nc-MeC/a-C:H coatings as well as hydrogen-free ones. Gählin et al. [14], pointed out that nearly 30 million car parts with PVD deposited nc-MeC/a-C coatings (mostly of nc-WC/a-C type) were delivered to the automobile industry in 2001 with an annual increase of 50%.

It was the aim of the present work to verify the effect of a series of particular multiplex treatments developed in the Lodz University of Technology on the tribological behaviour of a Ti6Al4V alloy, which has been first diffusion-hardened in a glow discharge plasma in Ar+O<sub>2</sub> atmosphere.

## 2. Experimental

Disks from Ti6Al4V alloy (1" diam. and 6 mm thick) have been used as the substrates. In some cases (i.e., for EDS analysis, nanoindentation or Raman spectrometry) thin 0,56 mm monocrystalline pure Si wafers were used. Moreover, for tribological characterisation of superhard (i.e., >40 GPa [15]) a-C

coatings deposited by pulsed cathodic arc deposition (PCAD) hard Vanadis 23 HS disks were used instead of the Ti6Al4V ones. The near-to-surface zone of the Ti6Al4V alloy disks was diffusion-hardened with interstitial oxygen atoms to a value of ~1000 HV0.1 in a manner described elsewhere [16]. After the hardening the disks were mirror-polished using 1 μm diamond paste.

### 2.1. Nanolaminate coating deposition

The nanolaminate coatings (TiC/a-C)<sub>x3</sub> and (TiN/a-C)<sub>x3</sub> were deposited in an industrial multipurpose coating unit URM 079 described elsewhere [1] and equipped with four independent cathodic arc sources (two filtered cathodic arc evaporation (FCAE) sources of continuous mode and two unfiltered ones of pulsed (PCAD) mode) and with one high-power medium frequency magnetron sputtering source for reactive magnetron sputtering (RMS). Before introducing them into the vacuum chamber the substrates were washed in warm water with detergent admixture, next in acetone in an ultrasonic bath and dried with compressed nitrogen of high purity. After air evacuation the substrates were first cleaned with high-energy argon ions (approx. 1.2 keV) and next a thin intermediate Ti layer (approx. 100 nm) was deposited using the FCAE method. A detailed description of substrate cleaning and intermediate Ti layer deposition was given in ref. [11]. The conditions of the FCAE and RMS deposition of the TiC or TiN sublayers or of hard a-C ones by means of PCAD in the nanolaminate coatings (TiC/a-C)<sub>x3</sub> or (TiN/a-C)<sub>x3</sub> are given in Table 1. In order to measure the hardness and modulus of elasticity of different types of coatings, thicker single PCAD a-C coatings or FCAE or RMS TiC or TiN ones were deposited as well by increasing the number of pulses in the carbon arc discharge, or, the time of continuous arc evaporation, or, of reactive magnetron sputtering, respectively.

### 2.2. Nanocomposite coatings deposition

#### Deposition of carbon-based nanocomposite coatings

The nanocomposite nc-CrC/a-C, nc-CrC/a-C:H, nc-TiC/a-C, nc-TiC/a-C:H and nc-WC/a-C coatings were deposited in a vacuum-chamber of a magnetron sputtering unit B90 described elsewhere [17] and equipped with four independent, medium frequency magnetrons placed symmetrically around a vertical axis of the chamber every 90 deg. For deposition of any of the nanocomposite coatings three of the four magnetrons were equipped with high purity (3N) graphite targets and only one with Ti, Cr or W target (respectively). Before introducing into the vacuum chamber the substrates were prepared in the same manner as in the case of deposition of the nanolaminate coatings (see Chapter 2.1). After evacuation the chamber and the specimens were first heated with infrared radiators to approx. 420K and next the specimens were submitted to glow-discharge cleaning during approx. 300s at the negative bias potential -1kV in a pure Ar atmosphere under a pressure of 4 Pa. After cleaning firstly a thin (approx. 50 nm thick) intermediate pure Ti or Cr or W layer (respectively) was deposited during approx. 300s at a power of

Table 1.

Deposition parameters of single layer and nanolaminate coatings by means of FCAE or PCAD methods

Designation	Type of coating	Deposition method	Reactive gas flow		Pressure during deposition	Source parameters		Time of deposition
			[sccm]			Current	Power	
			N <sub>2</sub>	C <sub>2</sub> H <sub>2</sub>	[Pa]	[A]	[kW]	[s]
A-TiN	TiN	FCAE	14	-	3.7x10 <sup>-3</sup>	55	1.65	5400
A-TiC	TiC		-	8	1.5x10 <sup>-3</sup>			
B-TiN	TiN	RMS	16	-	2.7x10 <sup>-1</sup>	4	3	5400
B-TiC	TiC		-	8		3.9	3	4800
C	a-C	PCAD	-	-	1.0x10 <sup>-3</sup>	Cathode potential	Impulses' frequency	Count of impulses
						[V]	[Hz]	-
						275	7	Up to 12000
Layers' sequence in nanolaminate (NL) coatings								
NL-1	(TiN/C) <sub>x3</sub>	Designation	1	2	3	4	5	6
			A-TiN	a-C	B-TiN	a-C	B-TiN	a-C
NL-2	(TiC/C) <sub>x3</sub>	Duration	A-TiC	a-C	B-TiC	a-C	B-TiC	a-C
			240 s	4500 imp.	120 s	4500 imp.	120 s	4500 imp.

Table 2.

Deposition parameters of carbon-based nanocomposite coatings using a RMS method

Type of coating	Gas flow		Magnetrons power		Pressure during deposition	Bias	Time of deposition	Coating's thickness
	Ar	H <sub>2</sub>	Cr or Ti or W target	3 x C targets*				
	[sccm]	[sccm]	[kW]	[kW]	[P]	[V]	[s]	[μm]
nc-CrC/a-C	30.8	-	0.23	3.64	0.40	-50	7 500	0.28
nc-CrC/a-C:H	17.7	5	0.2	3.66	0.40			0.65
nc-TiC/a-C	21.6	-	0.5	3.13	0.45		3 900	0.22
nc-TiC/a-c:H	17.4	15	0.3	3.08	0.43		3 900	0.43
nc-WC/a-C	14.2	-	1.15	3.35	0.33		21 200	0.36
nc-WC/a-C:H	24	12	0.3	4.2	0.55		4.6	

0.8 kW. In the next step a proper nanocomposite layer was deposited with all the four magnetrons working and at continuous rotation of the rotary table with specimens placed in the centre of symmetry of the system. The conditions of deposition of all the carbon-based nanocomposite coatings are given in Table 2.

**Deposition of nc-TiN/a-SiN nanocomposite coatings**

Thick nanocomposite nc-TiN/a-SiN coatings were deposited onto 1" diam. Ti6Al4V alloy. The coatings were deposited in a vacuum chamber with use of four rectangular magnetrons forming a closed unbalanced magnetic field (Fig. 1). Three of the four magnetron targets of thickness 9 mm were sintered from high purity Si and Ti powders at a relative mass fraction 1:16 and one target was manufactured from pure grade 1 Ti plate. The magnetron targets were powered with four synchronized medium frequency unipolar sinusoidal current sources of high power (~15 kW) and extreme voltage -1600 V modulated with an acoustic frequency, whereas the magnetrons' power was modulated using very short high pressure gas pulses at an infrasound frequency (~1 Hz) according to a newly developed technology of high density gas pulse plasma magnetron discharge [18] (Fig. 2). The mean magnetron discharge power density released during a single pulse

on an active part of a magnetron target surface was ~50 W·cm<sup>-2</sup> and a mean value of pressure of the reactive atmosphere (Ar + N<sub>2</sub>) during deposition was ~0.1 Pa. Temperature of specimens during deposition was ~ 800 K due to an indirect heating using a resistance



Fig. 1. Internal equipment of a vacuum chamber with four rectangular magnetrons forming a closed magnetic field configuration for magnetron sputtering (CFUBMSIP system) around a rotary heater with specimens

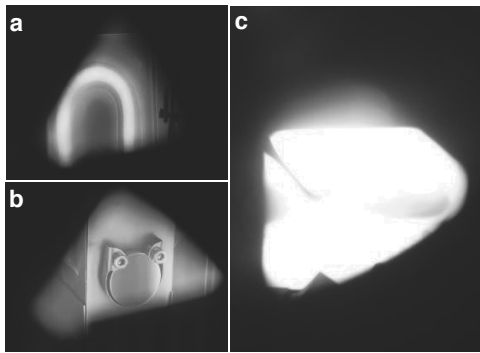


Fig. 2. Low density plasma in front of the magnetron target's surface (a) and in the vicinity of a specimen's surface (b) during a conventional magnetron sputtering and a high intensity plasma flash in front of the same specimen due to an instantaneous injection of a small volume of a gas mixture Ar+N<sub>2</sub> under high pressure (c) during deposition of a superhard nc-TiN/a-SiN nanocomposite coating

heater fixed to a rotary table (Fig. 1). Before a nc-TiN/a-SiN coating's deposition a thin (~80 nm) TiN interlayer was deposited for better adhesion by means of a reactive magnetron sputtering.

### 2.3. Coatings characterization

After deposition the coatings were characterized by EDS, OM, SEM, HRTEM, XPS, XRD, dynamic nanoindentation (for nano-hardness and nanomodulus measurement), Raman shift spectrometry, Daimler-Benz and ball-on-disk tests and scratch testing using a Rockwell indenter. In particular, the dry friction coefficient of the coatings was measured against a hard steel bearing ball of 5 mm diam. under a load of 10 N, at a constant linear velocity of 0.1 m·s<sup>-1</sup>, at a temperature (296 ± 2) K in static air of relative humidity (52 ± 2) %.

## 3. Results of coatings characterisation

The thickness of both nanolaminate NL-1 and NL-2 coatings, measured by means of optical interferometry or by SEM investigations, was equal to 0.4 μm (see also Fig. 4), whereas that of the single-phase FCAE or RMS ones (A-TiC, A-TiN, B-TiC and B-TiN) was greater and equal to 1.8 μm; 2.8 μm; 4 μm and 1.3 μm, respectively. The respective values for the nanocomposite coatings are given in Table 2 (see also Fig. 4). The thickness of a single PCAD a-C coating is 0.28 μm. The chemical compositions of the coatings were given as follows (in at.%): A-TiC(20/80), A-TiN(49/51); B-TiC(69/31); B-TiN(71/29). The chemical compositions of the nanocomposite coatings in at.% were as follows: (12.5/87.5); (18.5/81.5); (12.5/87.5); (5/95); (58/42) and (14.2/85.8) for nc-CrC/a-C, nc-CrC/a-C:H, nc-TiC/a-C, nc-TiC/a-C:H, nc-WC<sub>1-x</sub>/a-C and nc-WC<sub>1-x</sub>/a-C:H, respectively (without taking into account the hydrogen admixture in the hydrogenated coatings). An example of a XRD investigation is given in Fig. 5 and two spectra of the Raman shifts are given in Fig. 6. An example of the results of the HRTEM investigations of the nc-TiC/a-C nanocomposite nanostructure is given in Figs. 7 and 8.

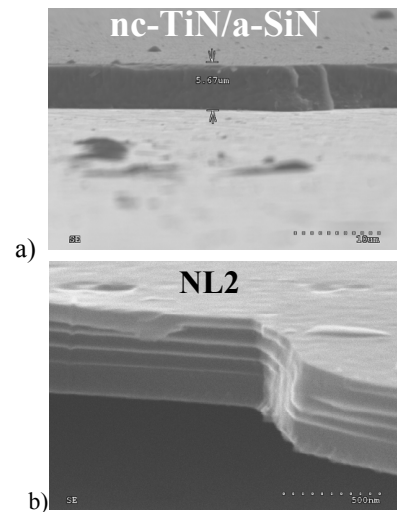


Fig. 3. Fracture of thick superhard nanocomposite nc-Ti/a-SiN coating on diffusion-hardened Ti6Al4V substrate (a) and of still harder NL-2 nanolaminate (TiC/C)<sub>3</sub> (b)

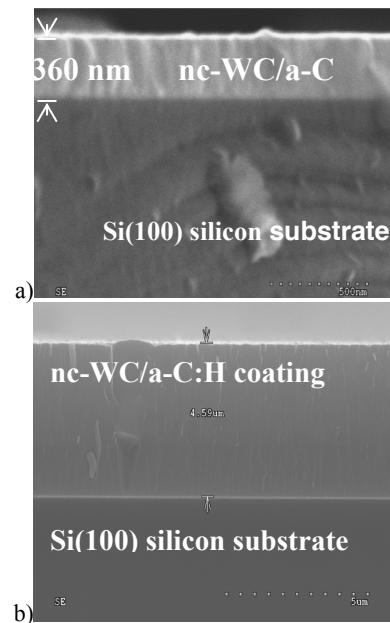


Fig. 4. Magnetron-sputtered nanocomposite coatings on monocrystalline Si (100) substrate: (a) hydrogen-free nc-WC<sub>1-x</sub>/a-C and (b) hydrogenated nc-WC/a-C:H of the thickness 0.36 μm and 4.6 μm, respectively, and good adhesion to the Si substrate

The microhardness values of the thick FCAE TiC and TiN coatings are given in Table 3. The results of dynamic measurements of nano-hardness as well as of nanomoduli of a-C (PCAD), NL-1, NL-2 as well as of all the nanocomposite coatings are given in Table 4 together with the resulting values of H/E (i.e., strain-to-failure). The results of the XPS investigation of chemical

Table 3.

Microhardness ( $\mu\text{H}$ ) measured under a load of 0.5 N of thick TiC and TiN coatings deposited by FCAE (A-TiC and A-TiN coatings) and RMS methods (B-TiC and B-TiN ones)

	A-TiC	A-TiN	B-TiC	B-TiN
$\mu\text{H}$ [GPa]	19	31	22	33

Table 4.

Nanohardness (nH) and nanomodulus (nE) of thin a-C, nanolaminate NL-1 and NL-2 and nanocomposite nc-WC/a-C, nc-TiC/a-C, nc-TiC/a-C:H, nc-CrC/a-C and nc-CrC/a-C:H coatings

	a-C	NL-1	NL-2	nc-CrC/a-C	nc-CrC/a-C:H	nc-TiC/a-C	nc-TiC/a-C:H	nc-WC/a-C	nc-WC/a-C:H	nc-TiN/a-SiN
nH [GPa]	33	45	53	14	13	15	12	20	17	47
nE [GPa]	270	440	480	200	180	210	150	250	200	560
H/E	0.12	0.10	0.11	0.07	0.07	0.07	0.08	0.08	0.085	0.084

Table 5.

Wear rate of Ti6Al4V alloy after different treatments as a result of dry sliding against steel 100Cr6 bearing-ball

Ti6Al4V as delivered	After diffusion hardening	Diffusion-hardened & coated with			
		a-C	NL-1	NL-2	nc-TiN/a-SiN
		$\times 10^{-15} \text{ m}^3 \cdot \text{N}^{-1} \cdot \text{m}^{-1}$			
~600	~100	0.51	0.38	0.22	32

bonds as a function of the time of cratering (with use of an Ar-ion gun) in depth from the surface of the NL-2 nanolaminate coating is shown in Fig. 9. The micrographs of the indents made using a Rockwell C indenter on the surface of two diffusion-hardened Ti6Al4V specimens with nc-CrC/a-C or nc-TiC/a-C coatings are shown in Fig. 10. The results of a ball-on-disk investigations of dry friction of several nanolaminate and nanocomposite coatings on diffusion-hardened Ti6Al4V alloy against a steel bearing-ball under a load of 10 N (and corresponding contact stress  $\sim 1.5$  GPa) are given in Fig. 11. The results of measurements of the volume wear rates of the coatings during a ball-on-disk tests are given in Table 5.

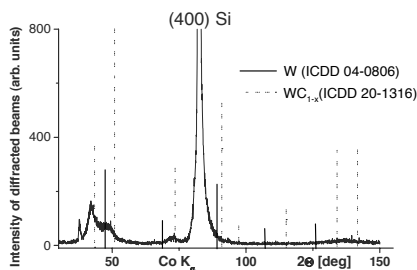


Fig. 5. X-ray diffraction profile of the nc-WC<sub>1-x</sub>/a-C coating on a mirror-polished (100) surface of a monocrystalline Si wafer

#### 4. Discussion of the results

It was found by means of the XRD phase analysis that both the nanolaminate NL-1 and NL-2 coatings as well as all the nanocomposite ones were quasi-amorphous except for the nc-WC<sub>1-x</sub>/a-C one which appeared to be apparently at least partially nanocrystalline (see Fig. 5). This finding corresponded well with a much higher atomic concentration of the tungsten atoms in this

coating in comparison with all the other nanocomposite coatings and with a much higher friction coefficient (see Fig. 11b). The latter was due to a much lower concentration of carbon atoms which were conducive to a lower friction and wear of rubbing surfaces. As a result of further investigations of the coatings' nanostructure using a transmission electron microscopy (TEM) as well as a high-resolution transmission electron microscopy (HRTEM) it was proved that all the nanocomposite coatings investigated in the paper were composed of nanocrystallites of transition metal carbides or nitrides embedded in an amorphous carbon or amorphous SiN matrix, respectively (see Fig. 7). The carbon-based nanocomposite as well as the nanolaminate coatings were characteristic of a very smooth surface and their Ra roughness parameter could be as low as 0.01  $\mu\text{m}$  (see Fig. 3b and Fig. 4).

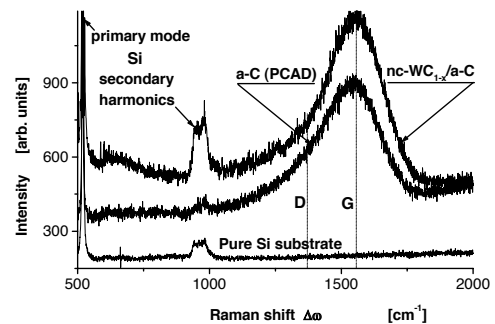


Fig. 6. Spectra of the intensity of the scattered laser light ( $\lambda = 514.5$  nm) as a function of the Raman shift  $\Delta\omega$  for three different materials: pure Si (100) substrate and two of the deposited coatings: a-C (PCAD) and magnetron sputtered nc-WC<sub>1-x</sub>/a-C. The positions of primary and secondary harmonics from Si-Si bonds (coming from the Si-substrate as well as of a disordered D-band and a graphite-type G one (coming from different carbon sp<sup>3</sup> and sp<sup>2</sup> hybridizations) are marked in the figure as well

The adhesion of the nanocomposite nc-MeC/a-C coatings to the diffusion-hardened Ti6Al4V substrate was good as well: the tests performed using the Daimler-Benz method gave the most frequently the value HF1 (see Fig. 10), and the second critical  $L_c$  II load from the scratch test using the Rockwell C diamond indenter was of the order of 30 - 60 N. Estimation of the adhesion of the nanolaminates NL-1 and NL-2 using the same D-B test gave the results much worse (HF3 and HF4) owing to, most likely, much

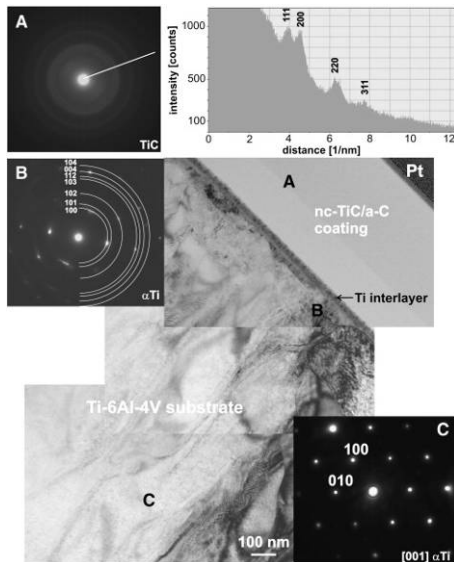


Fig. 7. TEM Microstructure of a thin ( $\sim 0.6 \mu\text{m}$ ) nc-TiC/a-C nanocomposite coating on enhanced oxygen diffusion hardened Ti6Al4V alloy and SAED patterns of the coating (insert A) as well as of different zones B and C of the Ti6Al4V substrate with corresponding SAED patterns. An intensity profile of the micrograph A along the line marked in the insert is given in the figure as well together with identification of diffracting planes of the grain C of the  $\text{Ti}_\alpha$  phase

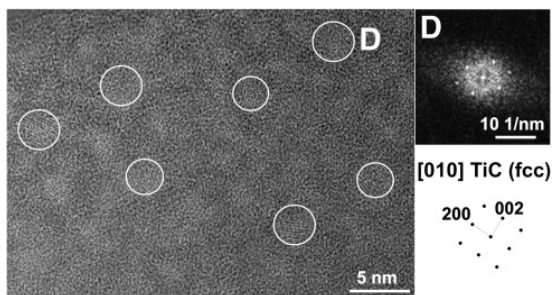


Fig. 8. HRTEM micrograph from a foil cross-section (obtained using FIB - a focused ion beam technique) of the nanocomposite nc-TiC/a-C coating on oxygen hardened Ti6Al4V alloy and a corresponding fast Fourier transform (FFT) of the electron diffraction pattern D calculated from the nanocrystalline area marked as D in the primary micrograph together with its identification below the D pattern (bottom right)

higher hardness and rigidity of these coatings (see Table 4) in comparison with the carbon-based nanocomposite ones, the hardness of which did not exceed 25 GPa and their Young's modulus was much lower as well (Table 4). Even though there were radial cracks around the indents in the coatings on the hardened Ti6Al4V substrate (Fig. 10) – no delamination was observed for the carbon-based nanocomposite coatings as thick as  $4.6 \mu\text{m}$  (see Fig. 4b).

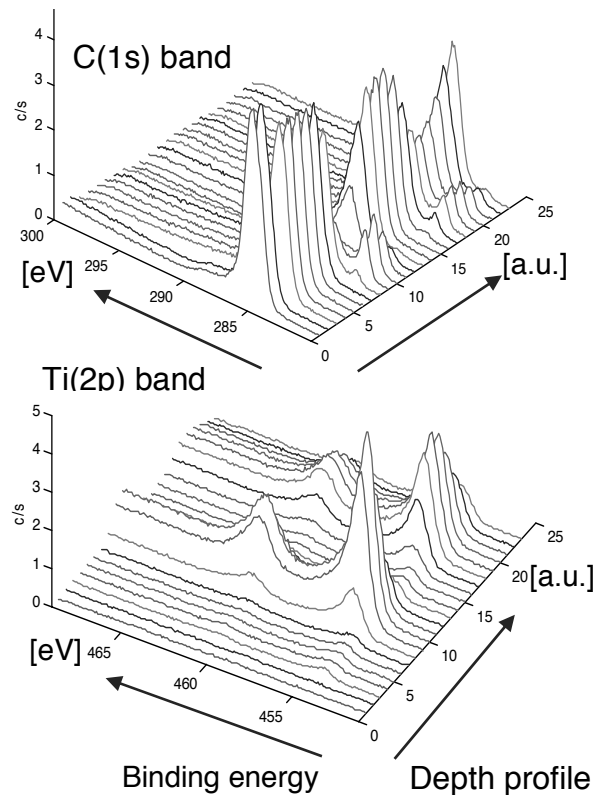


Fig. 9. Consecutive changes of the XPS C(1s) and Ti(2p) spectra in depth from the surface of the nanolaminate  $(\text{TiC/C})_{x3}$  coating on Ti6Al4V alloy registered during depth profiling with use of an  $\text{Ar}^+$ -ion gun

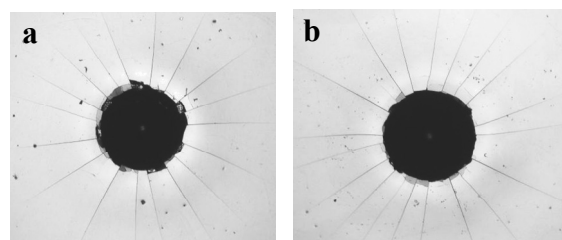


Fig. 10. Two indents of a Rockwell C diamond indenter after a Daimler-Benz test on the surface of diffusion-hardened Ti6Al4V alloy covered with a nanocomposite nc-CrC/a-C (the figure on the left) and nc-TiC/a-C coatings (the one on the right)

It is worth noting that the values of a “strain-to-failure” ratio  $H/E$  (hardness to the Young’s modulus) for a hard single amorphous PCAD a-C coating as well as for the superhard nanolaminates NL-1 and NL-2 were apparently higher than for all the nanocomposite coatings investigated in the work (Table 4). This was most likely due to increasing role of the interfaces in the nanocomposites in comparison with the nanolaminates or with a hard amorphous a-C monolayer.

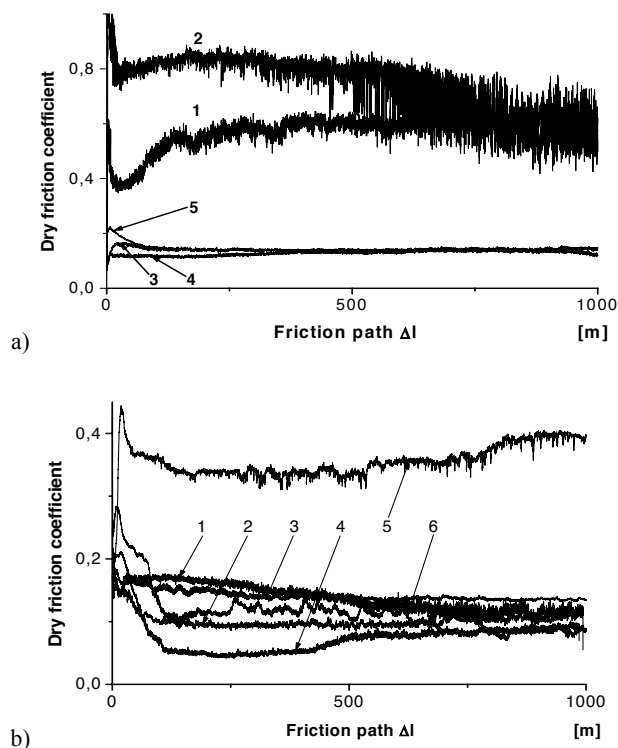


Fig. 11. Dry friction coefficient of a steel bearing-ball against Ti6Al4V. (a): 1 - substrate as delivered; 2 - diffusion hardened; 3, 4 - coated with superhard NL2 or NL1 nanolaminates, respectively; 5 - coated with hard a-C (PCAD); (b): diffusion-hardened Ti6Al4V substrate coated with 6 different nanocomposite coatings: 1 - nc-CrC/a-C; 2 - nc - CrC/a-C:H; 3 - nc-TiC/a-C; 4 - nc-TiC/a-C:H; 5 - nc-WC/a-C and 6- nc-WC/a-C:H

The alternating changes of the XPS intensities of the C1(s) and Ti2(p) bands in Fig. 9 corroborated well a stratified arrangement of the subsequent carbon and TiC layers in the NL-2  $(TiC/C)_{x3}$  nanolaminate. A characteristic feature of all the investigated carbon-based hard and superhard nanocomposite and nanolaminate coatings was a broad asymmetrical carbon-based maximum intensity of the Raman spectrum in the vicinity of  $1500\text{ cm}^{-1}$  as a result of superposition of two different types of hybridization of the C atoms: a regular  $sp^2$ -type (related to a G band in Fig. 6, characteristic for carbon bonds in, e.g., graphite) and a disordered one with different fraction of the  $sp^3$  hybridization characteristic for C-C bonds in diamond.

The very promising features of the nanocomposite (and nanolaminate) carbon-based coatings were their advantageous

tribological properties. First of all, a greater part of the nanolaminate and nanocomposite coatings characterized in the paper decreased the friction coefficient against a steel bearing-ball approximately one order of magnitude (see Fig. 11). At the same time the rate of their volume wear became several orders of magnitude smaller (Table 5). The sole exclusion from this behaviour made the nanocomposite nc-TiN/a-SiN coating, for which the dry friction coefficient against a ball-bearing 100Cr6 steel was as high as 0.8 (i.e., the same as that for as-delivered Ti6Al4V alloy - see Fig. 11a) and its wear rate during dry friction against steel bearing-ball is only 20 times less than that for a bare Ti6Al4V alloy. This relatively high wear rate of the nc-TiN/a-SiN coating and a high value of its dry friction coefficient was most likely due to a much higher value of the roughness parameter of this coating  $R_a \sim 0.1\ \mu\text{m}$  (see Fig. 3a). This result seemed to limit the scope of possible applications of superhard nanocomposite nc-TiN/a-SiN coatings deposited by means of the newly developed high density gas pulse plasma magnetron sputtering to protection of cutting tool rather than to friction reduction in tribological sliding couples.

It is worth to mention that due to a small radius of the friction track on a coated Ti6Al4V disk during a ball-on-plate test, the coatings along the total length of the friction path  $\Delta l=1000\text{ m}$  were submitted to  $\sim 1.6 \cdot 10^4$  stress cycles of an amplitude  $\sim 1.5\text{ GPa}$ , however no fatigue cracks were discovered on the tested surfaces.

It followed from Fig. 11 as well that in case of the carbon-based nanocomposite coatings, their hydrogenization decreased the friction coefficient in comparison with the hydrogen-free ones. Also it was observed a beneficial effect of the coatings’ hydrogenization on the adhesion of the coating to the Ti6Al4V substrate. This last statement needed, however, further experimental corroboration.

## 5. Conclusions

1. A series of different nanolaminate and nanocomposite coatings were successfully synthesized on the surface of a diffusion-hardened Ti6Al4V alloy using a number of hybrid multiplex treatments including a newly developed proprietary high density gas pulse plasma magnetron sputtering.
2. All the coatings were hard or superhard and were characteristic of a very low roughness  $\sim 0.01\ \mu\text{m}$  except for the nanocomposite nc-TiN/a-SiN coating, for which the roughness was much higher ( $\sim 0.1\ \mu\text{m}$ ).
3. The coatings adhered well to the surface of the diffusion-hardened Ti6Al4V alloy.
4. All the coatings decreased the dry friction coefficient against 100Cr6 ball-bearing steel, some of the coatings decreased that coefficient even more than one order of magnitude, except for the nanocomposite nc-TiN/a-SiN coating for which no decrease of the coefficient was found in comparison with Ti6Al4V alloy as delivered.
5. The hydrogenated nanocomposite coatings decreased the friction coefficient more effectively than the hydrogen-free ones.
6. It looked like that the value of a “strain-to-failure” ratio decreases with increasing fraction of the interfaces in the nanolaminate and nanocomposite coatings.

7. Some of the coatings decreased the wear coefficient during dry sliding to a value  $2 \cdot 10^{-16} \text{ m}^3 \cdot \text{N}^{-1} \cdot \text{m}^{-1}$  close to a value characteristic for lubricated sliding couples from constructional steels.
8. The coatings were highly resistant to fatigue at cyclic stress loadings of the amplitude up to 1.5 GPa.

## Acknowledgements

The Authors acknowledge the financial support from the Project KomCerMet financed from the funds of the European pool "National Cohesion Strategy" in the framework of the 7<sup>th</sup> EC FP "Operational Programme: Innovative Economy", subject priority 1, priority axis: Research and Development of Advanced Technologies, Activity 1.3: Supporting R+D projects carried into effect in scientific centres on the benefit of private entrepreneurs, Subactivity 1.3.1: Evolutionary Projects as well as from the MaMiNa Project of the 7<sup>th</sup> EU Programme PEOPLE, Marie-Curie Actions, Initial Training Networks (Contract No. 211536).

## References

- [1] B. G. Wendler, W. Pawlak, Low friction and wear resistant coating systems on Ti6Al4V alloy, *Journal of Achievements in Materials and Manufacturing Engineering* 26/2 (2008) 207-210.
- [2] A.F. Yetim, F. Yildiz, Y. Vangolu, A. Alasaran, A. Celik, Several plasma diffusion processes for improving wear properties of Ti6Al4V alloy, *Wear* 267 (2009) 2179-2185.
- [3] A.A. Voevodin, J.S. Zabinski, C. Muratore, Recent Advances in Hard, Tough, and Low Friction Nanocomposite Coatings, *Tsinghua Science and Technology* 10/6 (2005) 665-679.
- [4] S. Yang, D. Camino, A.H.S. Jones, D.G. Teer, Deposition and tribological behaviour of sputtered carbon hard coatings, *Surface and Coatings Technology* 124 (2000) 110-116.
- [5] A. Czyżniewski, Deposition and some properties of nanocrystalline WC and nanocomposite WC/a-C:H coatings, *Thin Solid Films* 433 (2003) 180-185.
- [6] B.G. Wendler, P. Nolbrzak, W. Pawlak, Adam Rylski, Structure and properties of  $\text{WC}_{1-x}/\text{C}$  coatings deposited by reactive magnetron sputtering on ASP2023 HSS steel and monocrystalline Si substrates, *Materials Engineering* 165-166/5-6 (2008) 655-657 (in Polish).
- [7] T. Zehnder, J. Patscheider, Nanocomposite TiC/a-C:H hard coatings deposited by reactive PVD, *Surface and Coatings Technology* 133-134 (2000) 138-144.
- [8] Y.T. Pei, D. Galvan, J.Th.M. De Hosson, C. Strondl, Advanced TiC/a-C:H nanocomposite coatings deposited by magnetron sputtering, *Journal of the European Ceramic Society* 26 (2006) 565-570.
- [9] J. Lin, J.J. Moore, B. Mishra, M. Pinkas, W.D. Sproul, Syntheses and characterization of TiC/a:C composite coatings using pulsed closed field unbalanced magnetron sputtering (P-CFUBMS), *Thin Solid Films* 517 (2008) 1131-1135.
- [10] G. Gassner, P.H. Mayrhofer, J. Patscheider, C. Mitterer, Thermal stability of nanocomposite CrC/a-C:H thin films, *Thin Solid Films* 515 (2007) 5411-5417.
- [11] W. Pawlak, B. Wendler, Multilayer, hybrid PVD coatings on Ti6Al4V titanium alloy, *Journal of Achievements in Materials and Manufacturing Engineering* 37/2 (2009) 660-667.
- [12] D. Batory, A. Stanishevsky, W. Kaczorowski, The effect of deposition parameters on the properties of gradient a-C:H/Ti layers, *Journal of Achievements in Materials and Manufacturing Engineering* 37/2 (2009) 381-386.
- [13] K. Włodarczyk, M. Makówka, P. Nolbrzak, B. Wendler, Low friction and wear resistant nanocomposite nc-MeC/a-C and nc-MeC/a-C:H coatings, *Journal of Achievements in Materials and Manufacturing Engineering* 37/2 (2009) 364-360.
- [14] R. Gåhlin, M. Larsson, P. Hedenqvist, Me-C:H coatings in motor vehicles, *Wear* 249/3-4 (2001) 302-309.
- [15] S. Vepřek, S. Mukherjee, P. Karvankova, H.-D. Männling, J.L. He, K. Moto, Limits to the strength of super- and ultra-hard nanocomposite coatings, *Journal of Vacuum Science and Technology A* 21/3 (2003) 532-544.
- [16] B.G. Wendler, T. Liśkiewicz, Ł. Kaczmarek, B. Januszewicz, D. Rylska, S. Fouvry, A. Rylski, M. Jachowicz, Diffusion Strengthening of Ti6Al4V Alloy in Ar + O<sub>2</sub> Glow Discharge Plasma, *Materials Engineering* 3/140 (2004) 681-685.
- [17] B.G. Wendler, M. Danielewski, K. Przybylski, A. Rylski, Ł. Kaczmarek, M. Jachowicz, New type AlMo-, AlTi- or Si-based magnetron sputtered protective coatings on metallic substrates, *Journal of Materials Processing Technology* 175 (2006) 427-432.
- [18] B.G. Wendler, J. Dora, I.F. Progalskiy, C. Siemers, W. Pawlak, A. Rylski, M. Makówka, P. Nolbrzak, K. Włodarczyk, A method of a high density gas pulse plasma magnetron sputtering, Patent application No. P-391523 submitted to the Polish Patent Office the 15<sup>th</sup> of June 2010.